



# Modeling the wave propagation in viscoacoustic media: An efficient spectral approach in time and space domain

Khemraj Shukla<sup>a, \*</sup>, José M. Carcione<sup>b</sup>, Reynam C. Pestana<sup>c</sup>, Priyank Jaiswal<sup>a</sup>, Turgut Özdenvar<sup>d</sup>

<sup>a</sup> Boone Pickens School of Geology, 105 Noble Research Center, OSU, Stillwater, OK, 74078, USA

<sup>b</sup> Istituto Nazionale di Oceanografia e di Geofisica Sperimentale(OGS), Borgo Grotta Gigante 42c, 34010, Trieste, Sgonico, Italy

<sup>c</sup> Federal University of Bahia(UFBA), Depto. de Física da Terra e do Meio Ambiente, Center for Research in Geophysics and Geology(CPGG), Salvador, Bahia, Brazil

<sup>d</sup> Wave Equations LLC, Cypress, TX, 77433, USA

## ARTICLE INFO

### Keywords:

Fractional derivative  
Attenuation  
Wave propagation  
Spectral methods

## ABSTRACT

We present an efficient and accurate modeling approach for wave propagation in anelastic media, based on a fractional spatial differential operator. The problem is solved with the Fourier pseudo-spectral method in the spatial domain and the REM (rapid expansion method) in the time domain, which, unlike the finite-difference and pseudo-spectral methods, offers spectral accuracy. To show the accuracy of the scheme, an analytical solution in a homogeneous anelastic medium is computed and compared with the numerical solution. We present an example of wave propagation at a reservoir scale and show the efficiency of the algorithm against the conventional finite-difference scheme. The new method, being spectral in the time and space simultaneously, offers a highly accurate and efficient solution for wave propagation in attenuating media.

## 1. Introduction

Seismic modeling is essential for various seismic processing steps, which spans from seismic imaging to reservoir characterization. In the entire range of applications, seismic modeling must follow two important criteria, accurate physics and numerical accuracy. It has been very common to solve the second-order scalar wave equation using a finite-difference approximation in the time and spatial domains for seismic imaging (Dablain, 1986; Etgen and Dellinger, 1989; Kelly et al., 1976; Alford et al., 1974) and inversion problem (Pratt and Worthington, 1990). In these studies, the authors did not consider to incorporate the attenuative nature of the medium, which accounts for the anelastic effect present in the subsurface.

Carcione et al., (Carcione et al., 1988a, 1988b) have modeled the attenuation effect on wave propagation by using memory variables. The wave propagation results in an augmented system of partial differential equations defining the evolution of these variables. On the other hand, Stekl and Pratt (Štekl and Pratt, 1998), have solved the acoustic wave equation in the frequency domain incorporating the effects of attenuation, but this approach results into a computationally intensive

process as it is required to solve a Helmholtz equation for each frequency.

In another approach Carcione et al., (Carcione et al., 2002), used the theory of Kjartansson (Kjartansson, 1979) to solve the scalar acoustic wave equation with the constraint of constant-Q at all frequencies. The effect of Q is incorporated in the form of a fractional power of the time derivative of the stress variable ( $\sigma$ ). Fractional time-derivative of stress variable  $\sigma$  at time  $t$  depends on all previous value of  $\sigma$ . This is the memory property of fractional derivative, describing the attenuation. Carcione et al. (2002) have solved the integral form of the fractional time-derivative (Caputo, 1969) by using the Grünwald-Letnikov and a central-difference approximations with first and second order accuracy, respectively. The consistency, stability and convergence of the scheme is discussed by Mainardi (Mainardi, 2010). The approach adopted by Carcione et al. (Carcione et al., 2002) is accurate in producing the desired effect but it is computationally intensive and constrained by the order of the accuracy.

To avoid the memory requirements of the fractional time operators, Carcione (Carcione, 2010), introduced the fractional Fourier pseudo-spectral method to compute Laplacian derivatives of non-integer order. This approach implies anelastic attenuation and velocity dispersion when implemented in wave equations. Following this methodology,

\* Corresponding author.

Email addresses: khemraj@okstate.edu (K. Shukla); jcarcione@inogs.it (J.M. Carcione); pestana.reynam@gmail.com (R.C. Pestana); priyank.jaiswal@okstate.edu (P. Jaiswal); turgut.ozdenvar@gmail.com (T. Özdenvar)

Carcione and co-workers simulated constant- $Q$  wave propagation in a series of papers (Zhu and Carcione, 2013; Carcione et al., 2016). In these works, authors use second-order finite-difference scheme in time to solve the time derivatives. Here, we solve the time evolution with the spectral rapid expansion method (REM) (Pestana and Stoffa, 2010), so that the solution is fully spectral, in the time and space domains, thus improving the accuracy and the computer efficiency.

## 2. Constant- $Q$ medium

The constant- $Q$  model (Kjartansson, 1979) is based on a creep function of the form  $t^{2\gamma}$ , where  $t$  is time and  $\gamma \ll 1$ . Kjartansson model is completely described by two parameters, namely the phase velocity at a reference frequency and  $Q$ . Thus, it is much simpler than any constant- $Q$  model, such as, for instance, the Kelvin-Voigt and Zener models (Carcione et al., 1988a, 1988b, 1988c) and mainly used in its frequency domain form. The relaxation function  $\psi(t)$  for constants- $Q$  model is given by (Kjartansson, 1979)

$$\psi(t) = \frac{M_0}{(1-2\gamma)} \left(\frac{t}{t_0}\right)^{-\gamma} H(t), \quad (1)$$

where  $M_0$  is a reference bulk modulus,  $\Gamma$  is the Euler Gamma function,  $t_0$  is a reference time,  $\gamma$  is a non-dimensional parameter and  $H(t)$  is the Heaviside function.

To derive the wave equation and its analytical solution in lossy media it is essential to have the complex modulus  $M(\omega)$  for relaxation function given in equation (1).  $M(\omega)$  is expressed as (Carcione, 2014, p. 72)

$$M(\omega) = \mathcal{F} [\partial_t \psi(\omega)], \quad (2)$$

where  $\mathcal{F}$  represent the Fourier transform and  $\partial_t$  the time derivative.

The modulus,  $M(\omega)$  is given by (Kjartansson, 1979)

$$M(\omega) = M_0 \left(\frac{i\omega}{\omega_0}\right)^{2\gamma}, \quad \gamma = \frac{2}{\pi} \arctan \frac{1}{Q} \quad (3)$$

where  $\omega_0 = 1/t_0$  is reference frequency,  $i = \sqrt{-1}$ , and the reference modulus  $M_0$  is expressed as

$$M_0 = \rho c^2 \cos^2 \left(\frac{1}{2} \arctan \frac{1}{Q}\right), \quad (4)$$

where  $\rho$  and  $c$  are the mass density and phase velocity, respectively (Carcione, 2014, p. 100).

In lossy media, the stress variable ( $\sigma$ ) is related to the time history of the strain ( $\epsilon$ ) via a convolution operator,

$$\sigma(\mathbf{x}, t) = \psi(t) * \partial_t \epsilon(\mathbf{x}, t), \quad (5)$$

where the symbol “ $*$ ” denotes time convolution. The frequency-domain representation of equation (5) is

$$\mathcal{F} [\sigma(\mathbf{x}, \omega)] = M(\omega) \mathcal{F} [\epsilon(\mathbf{x}, \omega)]. \quad (6)$$

Combining equations (5) and (6) and Newton's second law of motion, Carcione (Carcione, 2014, p. 101) derived the wave equation in a lossy medium as

$$\partial_t^\beta \sigma(\mathbf{x}, t) = \rho \left(\frac{M_0}{\rho}\right) \omega_0^{2-\beta} \nabla_\rho \sigma(\mathbf{x}, t), \quad (7)$$

where  $\nabla_\rho = \partial_x \left(\frac{1}{\rho} \partial_x \sigma\right) + \partial_z \left(\frac{1}{\rho} \partial_z \sigma\right)$  and  $\beta = 2 - 2\gamma$ .

Equation (7) has a fractional power in the time derivative term, which imposes a problem while computing the numerical solution because it requires to store the solution at all the previous time steps to compute the solution at the current time step (Podlubny, 1998;

Carcione et al., 2002; Caputo et al., 2011). To circumvent this computational issue, Carcione (Carcione, 2010), proposed an anelastic wave equation for constant- $Q$ , equivalent to equation (7), but with spatial fractional derivatives. The acoustic wave equation for uniform-density medium is given by (Carcione, 2010),

$$\partial_t^\beta \sigma(\mathbf{x}, t) = \omega_0^{2-\beta} c^{2\beta} (\partial_x^2 + \partial_z^2)^\beta \sigma(\mathbf{x}, t) + f(x, z, t), \quad (8)$$

where  $f(x, z, t)$  is the forcing function and  $\beta$  ( $1 \leq \beta \leq 2$ ) defines the extent of attenuation in the medium.

The equivalence between equation (7) and equation (8) can be easily proven by performing the dispersion analysis of a plane wave (Carcione, 2010). The constant  $Q$  – model shown by equation (8) provides the liberty of choosing the  $Q$  value in a direct way, unlike the models presented by Carcione et al., (Carcione et al., 1988a, 1988b, 1988c), where  $Q$  values are computed by relaxation times of the material.

## 3. Numerical scheme

### 3.1. Computation of fractional laplacian

To compute spatial derivatives with a fractional power in equation (8), a generalized form of pseudo-spectral method is used (Carcione 2007, 2010) and expressed as

$$(\partial_x^2 + \partial_z^2)^\beta \sigma(\mathbf{x}, t) = \text{FFT2D}^{-1} \left[ (-1)^\beta (k_x^2 + k_z^2)^\beta \text{FFT2D}(\sigma(\mathbf{x}, t)) \right], \quad (9)$$

where  $\text{FFT2D}(2\text{D}^{-1})$  are forward (inverse) Fourier operator and  $\mathbf{k} (k_x, k_z)$  is wavenumber vector.

In the present study, we have used direct-grid pseudo-spectral method to compute the spatial derivatives, which is a reasonable choice as equation (8) is scalar in nature. Unlike any finite-difference scheme, the pseudo-spectral method provides the optimal spatial accuracy for a given grid size, which substantially reduces the numerical errors such as grid dispersion. In addition to the pseudo-spectral method, spectral finite element method (SPECFEM) can also be used. The SPECFEM will provide better accuracy for complex geometries, but it comes with an aided computational complexity. Finally, the finite volume method (FVM) is also successfully used to compute the spatial-derivative with integer power (LeVeque, 2002), but extension of this method to compute the spatial operator with fractional power is not trivial. The FVM, being a low order method, is also constrained by its accuracy.

The implementation of direct-grid method for the heterogeneous form of equation (8) will produce the Nyquist error due to FFT operators being global in nature. To circumvent the Nyquist error in numerical solution, staggered-grid pseudo-spectral method (Ozdenvar and McMechan, 1996) is used to compute the spatial derivatives. In staggered-grid pseudo-spectral method, the spatial derivatives are computed at half-grid points using the even-based Fourier transform.

### 3.2. Computation of time derivative

The spatial derivative in equation (8) is computed by using the pseudo-spectral method, which provides very high accuracy and reduces numerical artifacts, resulting due to grid dispersion (Kosloff and Baysal, 1982; Fornberg, 1987). The high order accuracy of the pseudo-spectral method causes the total accuracy of the numerical scheme (in the time and the space domain) to be dependent on the accuracy of the time integration scheme. To achieve the high accuracy of the numerical scheme in the space and time domain simultaneously, it is essential to increase the accuracy of the time integration scheme.

It is not obvious to achieve the high order accuracy in computation of the time derivative and thus, the accuracy is confined to 2<sup>nd</sup> order

(using the finite-difference scheme), while modeling the acoustic (Alford et al., 1974; Dablain, 1986; Zhang et al., 2011) and the viscoacoustic (Carcione et al., 2010) wave propagation. In these studies, second-order finite-difference approximations were used for time operator, but a high-accuracy and high-order approximations, such as 4<sup>th</sup> order finite-difference scheme and pseudo-spectral schemes, are used for spatial operators. These approximation of time derivative operator can introduce the numerical error, resulting into the distortion of the shape of the wavelet and grid dispersion, especially, while using the 4<sup>th</sup> order finite-difference spatial operator. To avoid these numerical errors, a small time step ( $\Delta t$ ) must be taken, which in turn reduces the efficiency of the numerical scheme. Thus, combination of pseudo-spectral method (for the spatial derivative) and low-order finite-difference method (for the time derivatives) becomes slow while performing large-scale and high-frequency seismic modeling. Further, various improvements through the finite-difference scheme were proposed to alleviate the accuracy of time-derivative operator (Etgen and Dellinger, 1989; Soubaras and Zhang, 2008; Zhang and Zhang, 2009) but these schemes are based on the trade-off between efficiency and accuracy.

Kosloff et al., (Kosloff et al., 1989) proposed the rapid expansion method (REM) to compute the time integration more accurately and efficiently. Based on the work of Tal-Ezer et al., (Tal-Ezer et al., 1987), wherein a Chebyshev approximation for time marching is used (Kosloff et al., 1989), incorporated Chebyshev approximation of cosine operator (appears in the solution of wave equation) in REM. To achieve the computational efficiency from one-step REM (Kosloff et al., 1989), Pestana and Stoffa (Pestana and Stoffa, 2010) exploited the recursive property of Chebyshev polynomials and proved the efficiency and accuracy of seismic modeling.

Following the work of Pestana and Stoffa (Pestana and Stoffa, 2010), we will derive the REM for equation (8). Fourier transform of equation (8) can be written as

$$\frac{\partial^2 \hat{\sigma}(k_x, k_z, t)}{\partial t^2} = - \left( \omega_0^{2-2\beta} c^{2\beta} (-1)^{\beta-1} (k_x^2 + k_z^2)^\beta \right) \hat{\sigma}(k_x, k_z, t), \quad (10)$$

where  $\hat{\sigma}(k_x, k_z, t) = \text{FFT2D}(\sigma(x, z, t))$ .

Using the correspondence principle (Carcione, 2014, p. 145-146), the solution of equation (10) can be written as (Pestana and Stoffa, 2010; Zhan et al., 2012)

$$\sigma(t + \tau) = -\sigma(t - \tau) + 2 \cos(\phi \tau) \sigma(t), \quad (11)$$

where  $\phi^2 = \omega_0^{2-2\beta} c^{2\beta} (-1)^{\beta-1} (k_x^2 + k_z^2)^\beta$ .

In order to derive an efficient numerical scheme, it is required that  $\phi^2$  can be written as summations of multiplication of functions of  $x$  [ $f(x)$ ] and wave vector  $k$  [ $h(k)$ ]. Thus  $\phi^2$  is expressed as

$$\phi^2 = \sum_j f_j(\vec{x}) h_j(\vec{k}). \quad (12)$$

Equation (12) ensures that  $\phi^2 \sigma = \sum_j f_j(\vec{x}) \text{FFT}^{-1} \left( h_j(\vec{k}) \text{FFT}(\sigma) \right)$  and is satisfied by equation (10). Thus, our ultimate objective is to expedite the computation of cosine term in equation (8).

The cosine function in equation (11) can be expressed as (Kosloff et al., 1989)

$$\cos(\phi \tau) = \sum_{k=0}^M C_{2k} J_{2k}(R \tau) L_{2k} \left( \frac{i\phi}{R} \right), \quad (13)$$

where  $C_{2k}$  are expansion coefficients with  $C_0 = 1$ ,  $C_{2k} = 2$  for  $k > 0$ .  $J_{2k}$  represents the Bessel's function of order  $2k$  and  $L_{2k}(z)$  are modified Chebyshev polynomials.  $R$  is the parameters defining the criteria for truncating the summation in equation (13). In addition to this,  $R$  also

conditions the  $L_{2k}$  in such a way that arguments of  $L_{2k}$  falls in  $[-1, 1]$ , which is a strict requirement for computation of Chebyshev polynomials.  $R$  is equal to the maximum eigenvalue of operator  $\phi$  and given as

$$R = \omega_0^{1-\beta} c_{max}^\beta (-1)^{(\beta-1)/2} \sqrt{\left[ \left( \frac{\pi}{\Delta x} \right)^2 + \left( \frac{\pi}{\Delta z} \right)^2 \right]^\beta}, \quad (14)$$

where  $c_{max}$  is maximum velocity and  $\Delta x$  and  $\Delta z$  are spatial grid size.  $R$  evaluated from equation (14) is complex thus, an absolute value of  $R$  is to be considered during numerical implementation.

The sum in equation (13) converges exponentially for  $M > \Delta t R$  (Tal-Ezer, 1986), also presented in Appendix B. Though, we are free to choose any value of  $\Delta t$  but selection of  $\Delta t$  will decide the number of terms required to converge the summation in equation (13). Since cosine is an even function so equation (13) contains only even polynomials and thus, recursive property of Chebyshev polynomials can be used to compute the  $L_{2k}(z)$  efficiently. The  $L_{2k}(z)$  can be written as

$$L_{k+2}(z) = 2(1 + 2z^2)L_k(z) - L_{k-2}(z). \quad (15)$$

Solution of equation (15) can be computed recursively with base conditions of  $L_0(z) = 1$  and  $L_2(z) = 1 + 2z^2$ . The sequence of Chebyshev polynomials need to be computed at each time step of wave propagation.

#### 4. Results

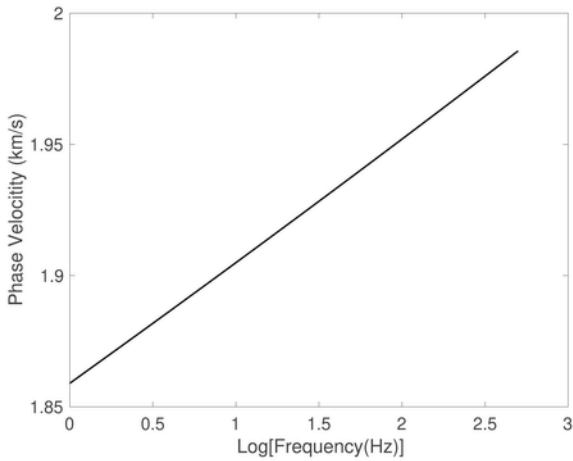
We consider  $c = 2$  km/s and  $\omega_0 = 2000$  Hz, representing the medium at an unrelaxed frequency. The unrelaxed frequency is defined by the frequency at which phase velocity achieves the maximum value. Alternatively, this can be also described by the fact that unrelaxed frequency corresponds to the maximum value of relaxation function (Carcione, 2014, pp. 90-91). Fig. 1 shows the phase velocity and attenuation versus frequency computed for equation (8). The dispersion is significant, with a velocity of 1.92 km/s at 15 Hz. Expressions for the phase velocity and the attenuation are given in Appendix C. In subsequent simulations the reference frequency  $\omega_0 = 2000$  Hz is considered, to produce the desired effect of attenuation on wave propagation.

Fig. 2 shows two snapshots at 500 ms, computed for  $Q = 5$  (Fig. 2a) and  $Q = 200$  (Fig. 2b). The simulation is based on a  $200 \times 200$  mesh, with square grid of size 10 m. The velocity of the medium,  $c = 2$  km/s is assumed. Equation (8) is solved, using the pseudo-spectral method to compute the spatial derivative, whereas the time stepping is performed using REM. A 2D point source (with a cylindrical spreading), multiplication of the Dirac function in space and the Ricker wavelet with a dominant frequency of 15 Hz in time, is used as the forcing function [ $f(x, z, t)$ ]. As postulated, the wavefront of the lossy case (Fig. 2a) travels slower than the wavefront of the quasi-elastic case (close to 2 km/s), shown in Fig. 2b.

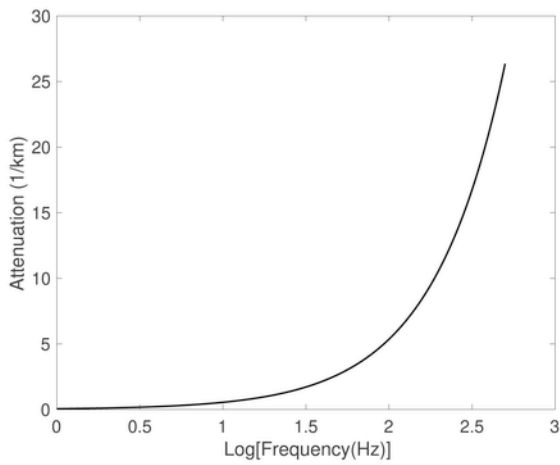
Fig. 3 represents the numerical simulation of equation (8), demonstrating the effect of spatially varying  $Q$  on wave propagation. Simulation parameters (except  $Q$ ) are same as those used in while generating Fig. 2. Fig. 3 clearly reflects the effect of  $Q$  on velocity and amplitude of the wave field. Wavefronts for  $Q = 10, 20$ , and 30 travel slower than those in the quasi-elastic (almost no attenuation) case ( $Q = 200$ ).

To prove the accuracy of the presented numerical scheme, we computed and compared the analytical and numerical solutions of equation (8). An analytical solution of equation (8) is derived by adopting the approach of Caputo et al., (Caputo et al., 2011) and shown in Appendix A. To compute the analytical and numerical solution, we use following forcing function,

$$f(t) = \left( a - \frac{1}{2} \right) \exp(-a), a = \left[ \frac{\pi(t - t_s)}{t_p} \right], \quad (16)$$



(a)



(b)

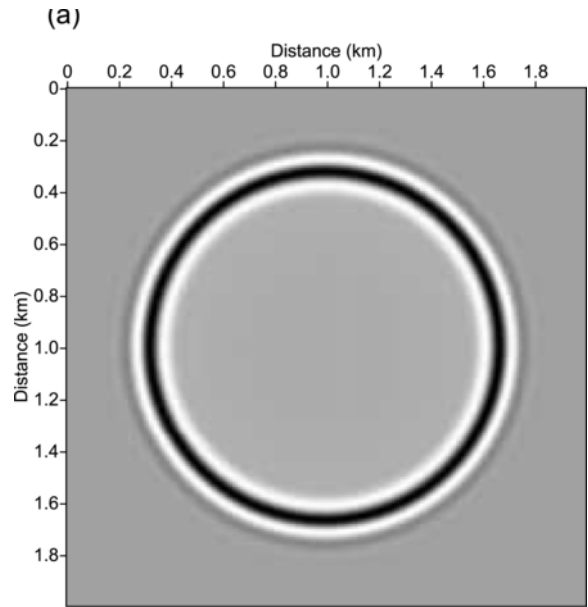
Fig. 1. (a) Phase velocity and (b) attenuation factor corresponding to  $Q = 30$ .

where  $t_p$  is period of wave and  $t_s = 1.4t_p$  represents delay in source. To compute the analytical solution, a frequency domain representation of equation (16) is required, which is expressed as

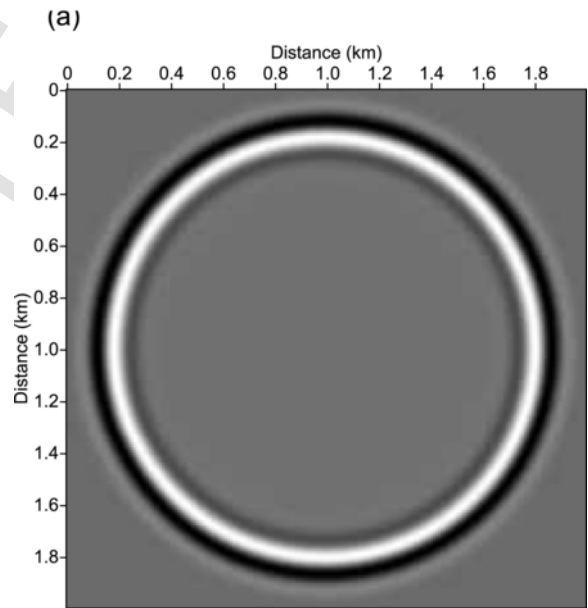
$$\begin{aligned}
 F(\omega) &= \left( \frac{t_p}{\sqrt{\pi}} \right) \bar{a} \exp(-\bar{a} - i\omega t_s), \bar{a} \\
 &= \left( \frac{\omega}{\omega_p} \right)^2, \omega_p \\
 &= \frac{2\pi}{t_p}.
 \end{aligned}
 \tag{17}$$

Fig. 4 represents a comparison between the analytical and the numerical solutions of equation (8) for  $Q = 5$ . The analytical and numerical solutions are computed at an offset of 60m for a source with dominant frequency of 15Hz and velocity  $c = 1527\text{m/s}$ . Fig. 4 clearly shows a good agreement between the numerical and analytical solution with an  $L^2$ -norm error of 0.4%.

Fig. 5 represents the snapshot of wave field, computed by solving equation (8) in an attenuative heterogeneous medium, comprising two layers of different velocity. Fig. 5a and b represent the snapshot of wavefield at 700ms for  $Q = 5$  and  $Q = 40$ , respectively. The simulation is based on  $400 \times 400$  mesh with grid size of 10m. The time re-



(a)



(b)

Fig. 2. Snapshots computed at 500ms using rapid expansion method for (a)  $Q = 5$  (b)  $Q = 200$ .

sponse of forcing function is a Ricker wavelet with the dominant frequency of 18Hz. The velocity ( $c$ ) of top and bottom layer is 1.5km/s and 2.0km/s respectively. The phenomena of the velocity varying with  $Q$  is very clear; in more attenuating medium ( $Q = 5$ , Fig. 5a) the traversed distance of wavefield is less in comparison to the less attenuating medium ( $Q = 40$ , Fig. 5b). In order to show the efficiency of REM over second-order finite-difference scheme, we compared the number of the Laplacian calculation required in finite difference and REM. In finite difference schemes, the time step for stable explicit-integration is computed using the Courant-Friedrichs-Lewy (CFL) condition. The CFL condition is the necessary condition, ensuring both the convergence and stability of numerical solution. Additionally, with the CFL the nu-

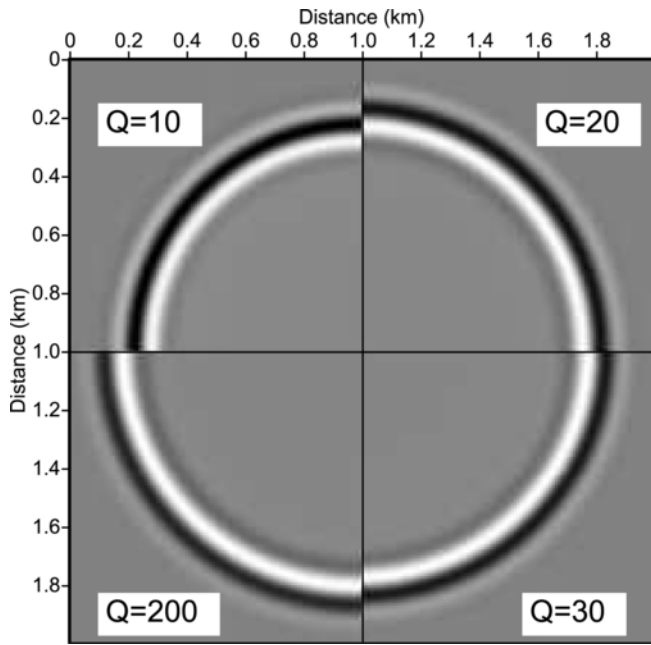
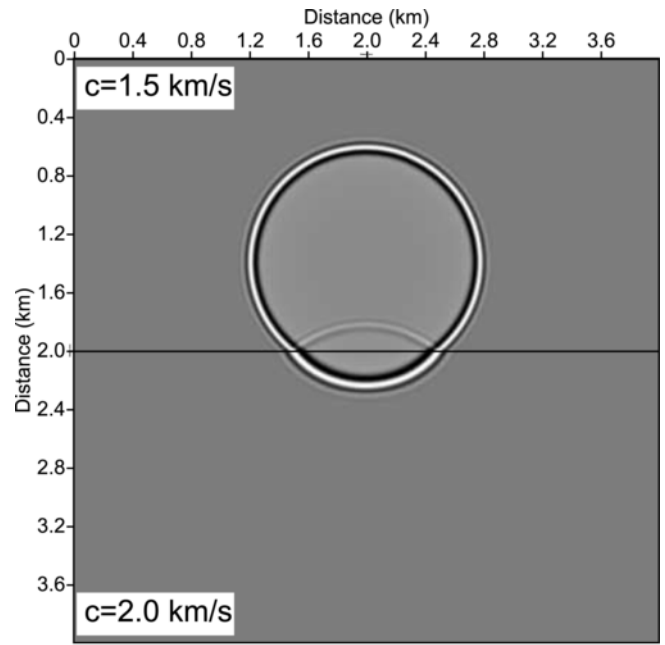


Fig. 3. A comprehensive view, showing the effect of the spatially varying  $Q$  ( $= 10, 20, 30,$  and  $200$ ) on the wave propagation, computed at  $500$  ms. It is to be noted that  $Q = 200$  represents a quasi-elastic medium.



(a)

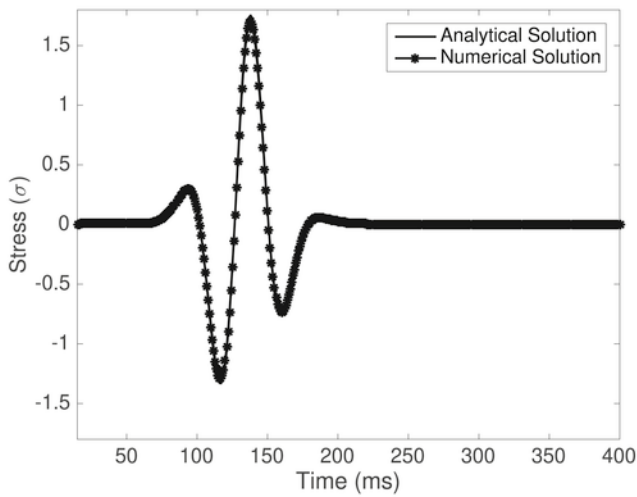


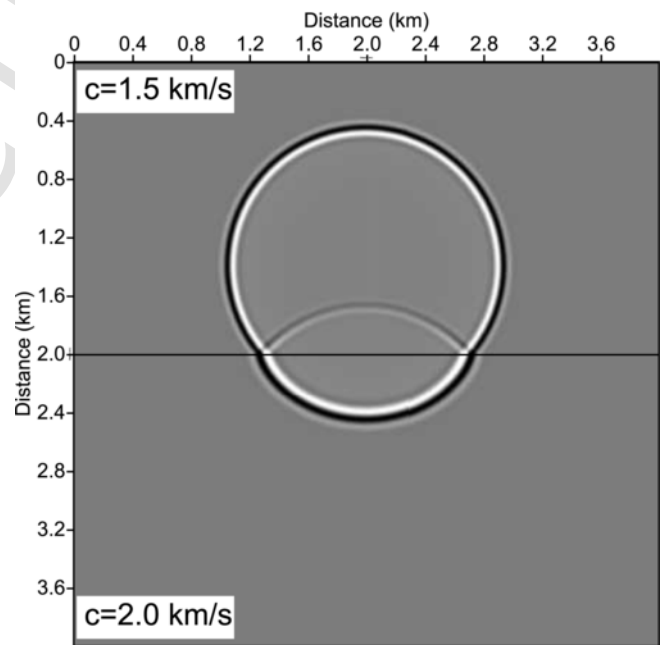
Fig. 4. A comparison between the analytical (solid line) and numerical (dots) solutions computed at  $Q = 5$ . The stress field ( $\sigma$ ) is computed at an offset of  $60$  m.

merical speed ( $\frac{t}{x}$ ) is always less than the physical speed of the wave. The CFL condition is given as

$$\alpha = \frac{c_{max} \Delta t}{\Delta x} \leq \left( \frac{\sqrt{2}}{\pi} \right), \quad (18)$$

where  $\Delta t$  is time step,  $\Delta x$  is grid size in space and  $c_{max}$  in maximum velocity.

For the finite-difference scheme, the number of the Laplacian is computed by dividing the maximum time of propagation ( $t_{max}$ ) with time step ( $\Delta t$ ), whereas the number of the Laplacian calculation for REM is  $> t_{max}R/2$ . For the case shown in Fig. 5, the number of the Laplacian calculation for the second-order finite-difference ( $\alpha = 0.2$ ) and the REM is 349 and 311, respectively. As the propagation time and the domain size are very small, the difference in the number of the



(b)

Fig. 5. Snapshots computed at  $700$  ms for variable velocity and constant density medium separated by an interface (equation using rapid expansion method for (a)  $Q = 5$  (b)  $Q = 40$ ).

Laplacian computation is not substantial though for the long simulation, the difference is very evident and shown in the subsequent section of the paper.

Numerical solution of equation (8) is computed for a large synthetic reservoir model, containing a gas chimney. The P-wave velocity (Fig. 6a) and Q model (Fig. 6b) is adopted from Zhu et al., (Zhu et al.,

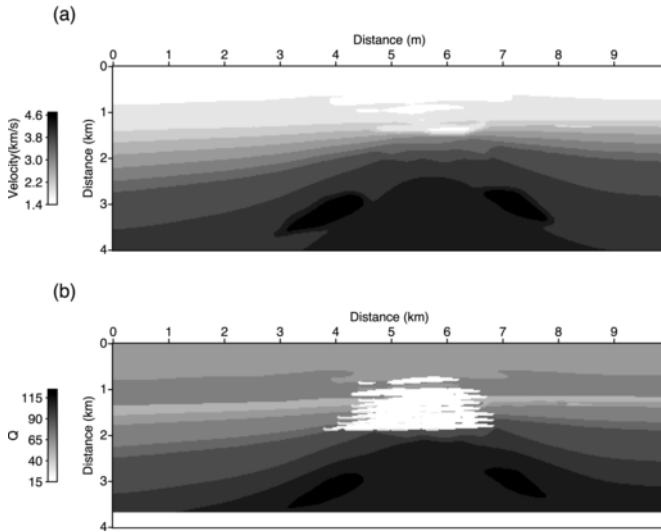


Fig. 6. Large scale synthetic reservoir model with (a) P-wave velocity and (b) Q model.

2014). In this model, the gas chimney is differentiated from the surrounding by a low value of velocity (Fig. 6a) and  $Q(\approx 15)$  (Fig. 6b). The velocity and Q models comprise 398 and 161 grid points in the x- and the z-direction, respectively. The grid spacing in both the direction is 25 m ( $dx = dz$ ). In the model, P-wave velocity varies from 1500 m/s ( $c_{min}$ ) to 4500 m/s ( $c_{max}$ ), which guarantees a max frequency of propagation ( $c_{min}/2\Delta x$ ) to be bounded below by the 30 Hz. A Ricker point source of 18 Hz central frequency is used as a forcing function. Fig. 7a represents the snapshot of stress-field ( $\sigma$ ) at 1.5 s with the Q model (Fig. 6b) incorporated in the computation. To show the effect of Q on the wave propagation, the numerical solution of equation (8) is also computed for a lossless medium. A lossless condition is achieved by considering  $\beta = 1$  in equation (8). Fig. 7b represents the snapshot of the wave field at 1.5 s for the lossless medium. A comparison between Fig. 7a and b reflects the fact that the dispersion due to the rheology of the model is incorporated accurately.

Fig. 8a and b represent the shot gathers in a lossy (corresponding to simulation shown in Fig. 7a) and lossless (corresponding to simulation shown in Fig. 7b) medium, respectively. To show the effect of Q on shot gathers, a comparison between amplitude spectra of Fig. 8a and b

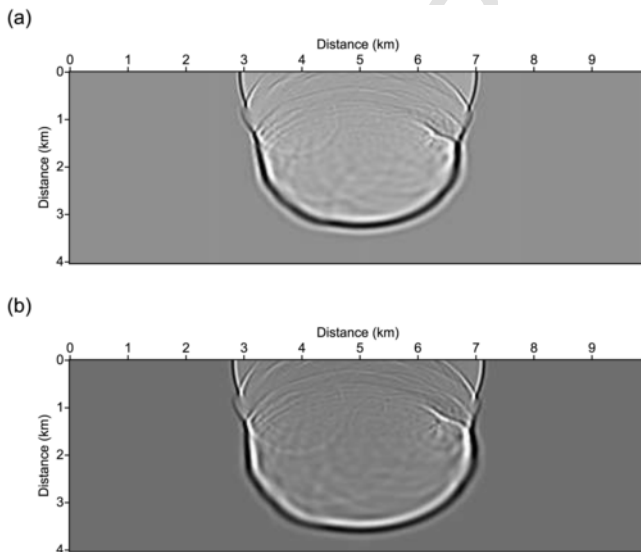


Fig. 7. Wave field simulation for a reservoir model (a) Snapshot of the wave field at 1.5 s with Q – and (b) wave field snapshot computed at 1.5 s with out Q – (lossless medium).

is shown Fig. 8c. Fig. 8c clearly shows the effect of attenuation on the amplitudes. As expected, the effect of attenuation is more evident at high frequencies, which is reflected by the steeper rate of decay in amplitude in lossy case than in lossless case. The dominant frequency is  $\approx 14.5$  Hz for both the cases. Fig. 8d contains a comparison between traces extracted at 250 m offset from the source. The effect of attenuation is clearly reflected in the amplitude and phase shifts (a shift in time) between the traces.

A comparison between the number of the Laplacian calculation required for REM and the finite-difference scheme, is shown in Table 1. Table 1 proves the fact that for all cases of  $\alpha$  and frequency, the REM is more efficient than the second-order finite-difference scheme.

A representative spectrogram (time-frequency) analysis of shot gathers, computed in the lossy (Fig. 9a) and the lossless media (Fig. 9b), is shown in Fig. 9. The spectrogram essentially calculate the short-time Fourier transform of the trace resulting into the amplitude at time-localized frequency. The basic reason behind these computation is to represent the distribution of the amplitude and phase (represented in term of time on y – axis) at a fixed time and for an entire frequency range (x – axis).

Fig. 9a and b represent the time-frequency analysis for a trace for an offset of 750 m in the lossy and the lossless media, respectively. It is worth to note that in a lossy media (Fig. 9a) the onset of dominant power of the signal is delayed ( $>0.4$  s) in comparison to that in lossless medium (Fig. 9b), which starts at  $\approx 0.4$  s. Thus, this time difference also confirms with the phase difference in attenuative media, as reported by (Carcione, 2010). Fig. 9a also shows that in lossy media, the variation of the amplitude with the frequency and time is more notable than in the lossless media (Fig. 9b).

## 5. Discussion

The implementation of the REM to compute the time derivative operator in equation (8), provides freedom in choosing the size of time step  $\Delta t$  (as shown in Figs. 2–9) with an increased accuracy in the numerical solution. The efficiency along with accuracy achieved from the REM will be very useful in various seismic imaging algorithms. In particular, the reverse time migration (RTM) algorithm which requires two-way solutions of the wave equation.

In another in-line study Sun et al., (Sun et al., 2015), computed the numerical solution for viscoacoustic equation, described by the fractional space derivatives with constant  $-Q$ , using a low rank approximation method (Fomel et al., 2013). The method of the low rank approximation does not impose any constraint on the size of  $\Delta t$ . Sun et al., (Sun et al., 2015) use the constitutive equations of Zhu and Harris (Zhu and Harris, 2014), which are based on the approximation of freezing-unfreezing theory of heterogeneous medium (Stein, 1999). They approximated the wave equation in the constant  $-Q$  medium using four Laplacians and two of them with the fractional order. Numerical solution of such equations will require four 2D FFT operations at each time step. However, in present study we just require two (one forward and one inverse) 2D-FFT operation at each time step. Thus a comparison between the efficiency of numerical scheme presented in this paper with the study carried out by Sun et al., (Sun et al., 2015) will not be appropriate.

To show the efficiency of the algorithm, we have analyzed the numerical scheme using the approach of basic algorithmic-complexity (Cormen et al., 2009). To compute the spatial operator in 3D, we require six runs of the FFT algorithm (three forward and three inverse). The computational complexity of one run of the FFT algorithm is  $\mathcal{O}(n \log n)$ , with  $n$  being the total number of nodes, used to discretized the domain in x, y and z directions. Thus the time complexity (2D or 3D), for computation of spatial derivatives is  $\mathcal{O}(n \log n)$ . Any algorithm with the complexity of  $\mathcal{O}(n \log n)$  suggests that the run time

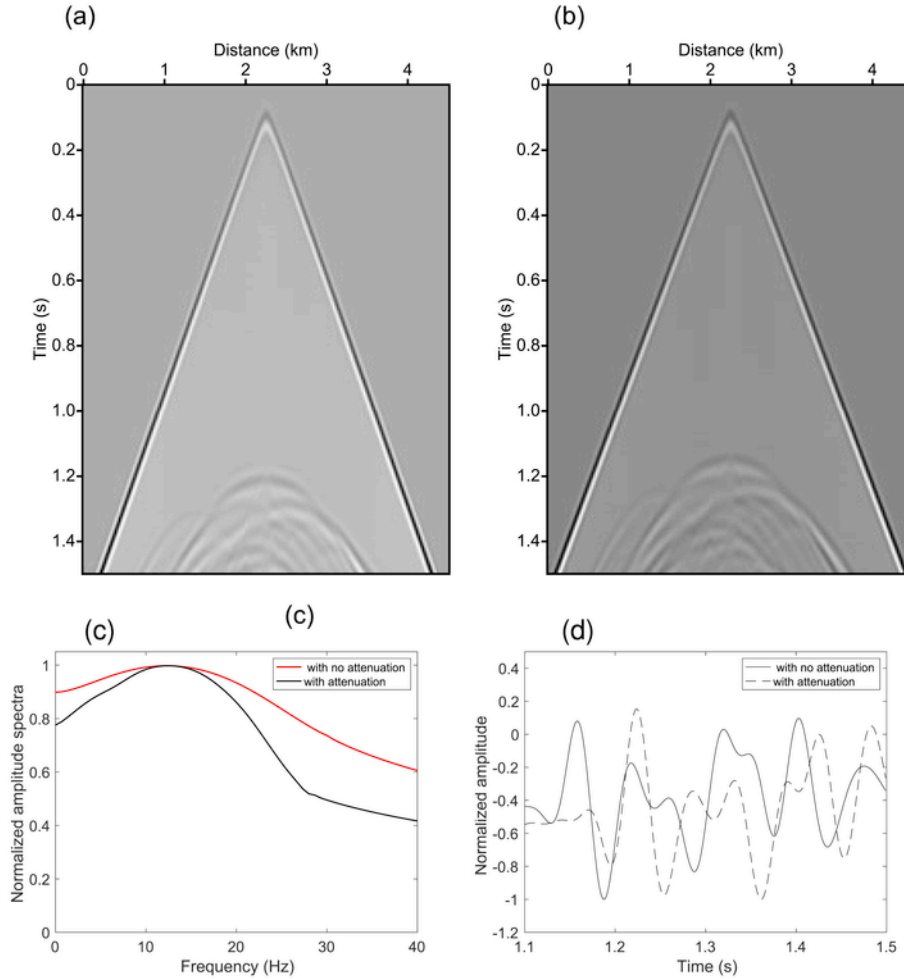


**Fig. 8.** Shot gathers extracted from simulations shown in Fig. 7a and b. Shot gather in a (a) lossy medium (b) lossless medium and (c) a comparison between normalized amplitude spectra of (a) and (b), and (d) pressure seismograms at 250m from the source location extracted for lossy and loss-less medium. The wave equation involves a fractional power of the Laplacian for the lossy case.

**Table 1**  
Number of Laplace calculations using second-order finite-difference (FD<sub>L</sub>) and REM (REM<sub>L</sub>), with maximum time of propagation,  $t_{max} = 1.5$  s.

$\alpha$	Freq. (Hz)	$\Delta x$ (m)	$\Delta t$ (s)	FD <sub>L</sub>	REM <sub>L</sub>
0.4	15.0	25.0	0.00217391	690	613
0.2	15.0	25.0	0.00434783	1380	613
0.4	45.0	15.0	0.00130435	1150	1022
0.2	45.0	15.0	0.00260870	2300	1022

grows slowly as  $n$  increases in comparison to algorithms with exponential and quadratic complexity. The time complexity for computing the time derivative is dominated by evaluation of the modified Chebyshev polynomials in equation (13). Since, we have used the recursive approach to compute the modified Chebyshev polynomials, the time complexity for the computation of the time derivative would be  $\mathcal{O}(M)$ . Thus, at each time step, the total computational complexity would be  $\mathcal{O}(M) + \mathcal{O}(n \log n)$ . Fig. 10 shows a comparison between the theoretical run time, described by  $\mathcal{O}(M) + \mathcal{O}(n \log n)$  and actual run time, computed for a 2D case. The run times are plotted against number of grid points in one direction. The run times are computed on a single node machine, comprising MacBookPro 2018 laptop with 8 cores and 2.3 GHz clock frequency. The comparison clearly shows a very good agreement between the theoretical and actual runtime, considering the fact that the code is not optimized, substantially.

As confirmed by Fig. 10, it can be concluded that the efficiency of the presented numerical scheme will be primarily dominated by the scalability of the FFT algorithm on a multinode architecture with a distributed memory hierarchy. The FFT has been already proven to be a strong scale algorithm (Pippig, 2013), which guarantees strong scalability of the presented numerical scheme on a multinode machine.

### 6. Conclusions

We have simulated the wave equation in attenuative media, efficiently and accurately, by implementing the REM and pseudo-spectral method to compute the time and fractional spatial derivatives respectively. Various computational experiments reflect the fact that the proposed efficient numerical scheme accurately incorporates the velocity dispersion, which is caused by  $Q$ . A comparison between the analytical and the numerical solutions shows a very good agreement. Numerical simulation for large scale reservoir model, shows a substantial efficiency of REM over second-order finite-difference scheme. We also presented the efficiency of our code by comparing the theoretical and actual run times, which shows a very good agreement.

### Computer code availability

To accelerate the dissemination and adoption of presented method in the wider community, we have made the entire project open source

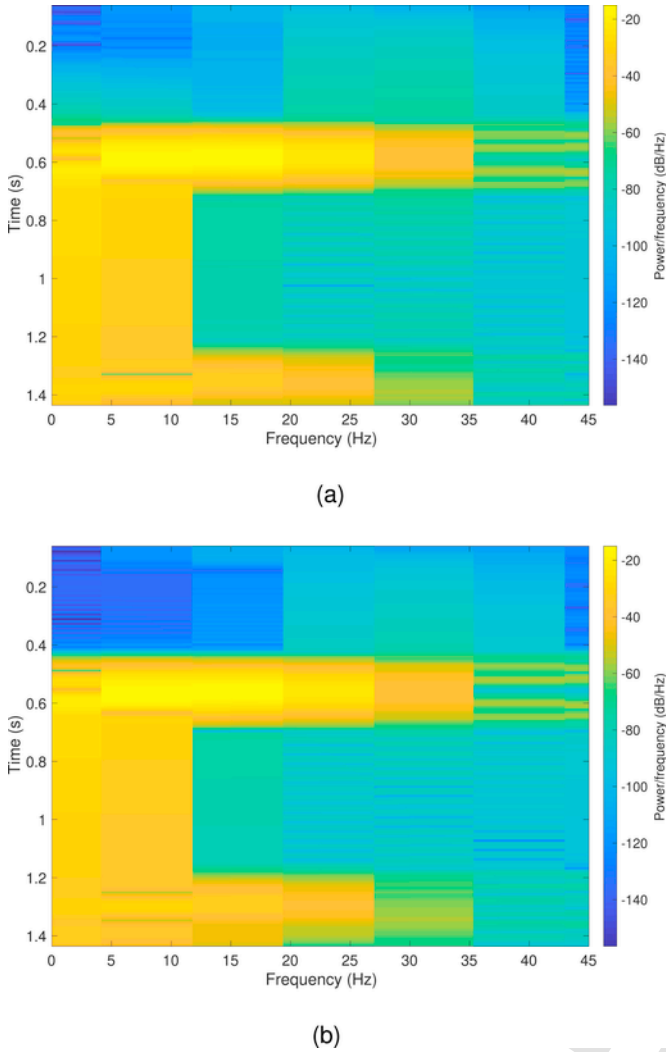


Fig. 9. Spectrogram or time-frequency plot of shot gather in (a) lossy medium (Fig. 8a), (b) lossless medium (Fig. 8b). Spectrogram is computed for a trace at an offset of 750 m.

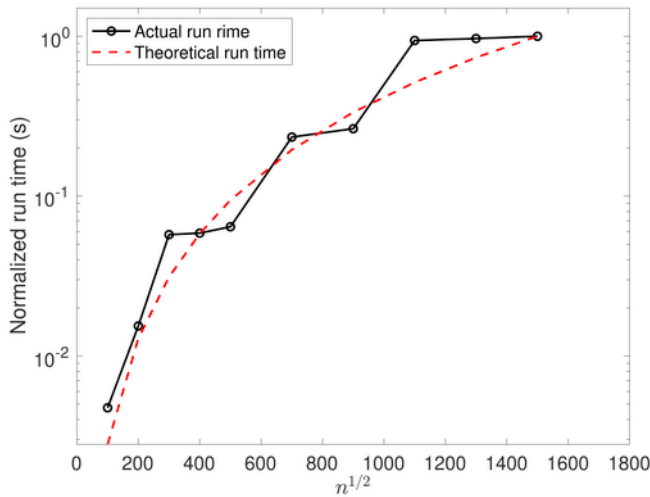


Fig. 10. A comparison between the theoretical and actual run time of the code written in the current work.

under the permissive MIT License. The code is hosted at [https://github.com/rajexplo/REM\\_COMPUTER\\_GEOSCIENCE](https://github.com/rajexplo/REM_COMPUTER_GEOSCIENCE). The code is written FORTRAN90 language and collaboratively developed by authors of the current paper. This code requires a third party library FFTW, extensively used for Fast Fourier transformation. This code is tested on MacBookPro 2018 laptop with 8 cores and 2.3GHz clock frequency. GNU compiler (gfortran) is used to compile and link the code. This code originally produces Fig. 5a and b presented in the current manuscript and just represent a prototype implementation of presented algorithm. For any question please contact at email address of corresponding author of the current manuscript.

**Contribution from authors**

- Author 1: Coded and derived the formulations; wrote the manuscript; incorporated the corrections and suggestions from all the coauthors.
- Author 2: Provided an idea for wave propagation in viscoacoustic media, helped in formulation of core idea, computing the analytical solution in attenuative media and helped the first author in coding the various parts of algorithm and rigorously corrected the manuscript.
- Author 3: Provided the basic foundation of REM, helped in coding the REM and provided vital inputs while correcting the manuscript.
- Author 4: Provided the idea of applying the presented algorithm for a large chimney model, helped in computing the spectrogram, and corrected the manuscript.
- Author 5: Rigorously corrected the manuscript, helped in corroborating the results and framing the discussions.

**Acknowledgements**

We thank Editors Prof. Dario Grana and Dr. Sjoerd, and three anonymous reviewers for very useful comments. Authors would like to acknowledge OGS, Italy for hosting KS at various occasions. KS would like to acknowledge Sundeep Sharma, Devon Energy, for various discussions and proofreading the manuscript. This is Boone Pickens School of Geology, Oklahoma State University, contribution number 2019-101.

**Appendix D. Supplementary data**

Supplementary data to this article can be found online at <https://doi.org/10.1016/j.cageo.2019.01.022>.

**Appendix A Green's function and analytical solution**

Equation of motion for wave propagation in anelastic media is expressed as (Carcione, 2014, p. 101)

$$\partial_t^{2n} = \frac{1}{\rho} \cdot \sigma. \tag{A.1}$$

Stress-strain relation in anelastic medium is expressed as

$$\sigma = \rho b \partial_t^{2-\beta} u + f, \tag{A.2}$$

where  $b = \left(\frac{M_0}{\rho}\right) \omega_0^{-2\gamma}$ . Substituting equation (A.2) in equation (A.1) we get

$$\partial_t^{2n} = b \partial_t^{2-\beta} u + \frac{f}{\rho}. \tag{A.3}$$

Taking Fourier transform of equation (A.3)

$$(i\omega)^{2n} = b(i\omega)^{2-\beta} u + f. \tag{A.4}$$

Using equation (8),  $b(i\omega)^{2-\beta} = M(\omega)$ , we rewrite equation (A.3) as

$$'''' + p^2'' = -\frac{f}{M(\omega)}, \quad (\text{A.5})$$

where  $p = \frac{\omega}{v_c}$  is wave number and  $v_c = \sqrt{\frac{M(\omega)}{\rho}}$  is complex phase velocity.

If  $v_c$  is real the medium is lossless. Solution to lossless acoustic equation  $(\Delta + p^2)G = -8\delta(r)$  is the Green function  $G$  (Carcione, 2007) and can be expressed as

$$G(x, y, x_0, y_0, \omega, c_0) = -2iH_0^{(2)}\left(\frac{\omega r}{c_0}\right), \quad (\text{A.6})$$

where  $c_0$  is real velocity in lossless media,  $H_0^{(2)}$  is zero order Henkel function of second kind. Coordinate pair  $(x_0, y_0)$  is location of source and  $r = \sqrt{(x-x_0)^2 + (y-y_0)^2}$ . (Caputo et al., 2011) computed anelastic solution by invoking the correspondence principle (Bland, 1960). According to the correspondence principle, solution in lossy media can be obtained by substituting  $c_0$  in equation (A.6) with  $v_c$ . Thus Green function for strain is

$$G_\epsilon = \frac{G}{M(\omega)}. \quad (\text{A.7})$$

Since  $\Delta G = -p^2G$  away from the source and  $\sigma = M(\omega)\epsilon$ , then Green's function for the stress can be expressed as

$$G_\sigma = M(\omega)G_\epsilon = -p^2G. \quad (\text{A.8})$$

To ensure the inverse Fourier Transform of Green's function to be real, we will set  $G(-\omega) = G^*(\omega)$ , where \* is complex conjugate. Thus the frequency domain solution for stress is given by  $\sigma(x, y, x_0, y_0, \omega) = \frac{1}{8}G_\sigma(\omega)f(\omega)$ , where  $f(\omega)$  is frequency domain representation of  $f(t)$ . As Henkel function has singularity at  $\omega = 0$ , we will assume  $G(\omega = 0) = 0$ .

## Appendix B Convergence and stability of scheme

We prove the convergence criteria of  $M > \Delta tR$  for series in equation (13). We rewrite 13 as

$$H_M(\phi't) = \sum_{k=0}^M C_{2k} J_{2k}(R't) L_{2k}\left(\frac{i\phi}{R}\right). \quad (\text{B.1})$$

The accuracy of  $H_M(\phi\Delta t)$ , a polynomial approximation, is defined by its asymptotic rate of convergence as  $M \rightarrow \infty$ . Consider the interval  $[m_0, \infty)$ , where the asymptotic behavior of equation (B.1) is defined. Thus to a prescribed accuracy, the minimal  $M \in [m_0, \infty)$ , should be  $> m_0$  to resolve all the Fourier modes. This is a necessary and sufficient condition as proven by (Tal-Ezer, 1986). Now we can derive the value of  $m_0$  for equation (B.1). It is a well known fact that the Bessel's function of order  $k$ , defined for a variable  $x$  as  $J_k(x)$ , converges to zero exponentially fast if  $k > x$  (Abramowitz and Stegun, 1972). Thus to resolve all the Fourier modes the interval of asymptotic behavior would be  $[x, \infty)$ , with  $m_0 = x$ . Thus, it proves that  $H_M(\phi\Delta t)$  will converge exponentially if  $k > \Delta tR$ .

## Appendix C Phase velocity and attenuation

The analysis of the propagation characteristic of the medium, defined by equation (8), is performed. The phase velocity ( $v_p$ ) and attenuation factor ( $\alpha$ ), in a medium of constant properties, for a plane wave, defined by  $\sigma = \exp[i(\omega t - k_x x - k_z z)]$ , are

$$v_p = \left[ \cos\left(\frac{\pi\gamma}{2}\right) \right]^{-1} \left( \frac{\omega}{\omega_0} \right) c \quad (\text{C.1})$$

$$\alpha = \frac{\omega}{c} \left( \frac{\omega_0}{\omega} \right)^\gamma \sin\left(\frac{\pi\gamma}{2}\right). \quad (\text{C.2})$$

## References

- Abramowitz, M., Stegun, I., 1972. Handbook of Mathematical Functions. dover, new york.
- Alford, R., Kelly, K., Boore, D.M., 1974. Accuracy of finite-difference modeling of the acoustic wave equation. *Geophysics* 39 (6), 834–842.
- Bland, D., 1960. The Theory of Linear Viscoelasticity. Pergamon Press.
- Caputo, M., 1969. Elasticita e dissipazione, Zanichelli.
- Caputo, M., Carcione, J.M., Cavallini, F., 2011. Wave simulation in biologic media based on the Kelvin-Voigt fractional-derivative stress-strain relation. *Ultrasound Med. Biol.* 37 (6), 996–1004.
- Carcione, J.M., 2007. Wave Fields in Real Media: Wave Propagation in Anisotropic, Anelastic, Porous and Electromagnetic Media, vol. 38, Elsevier.
- Carcione, J.M., 2010. A generalization of the Fourier pseudospectral method. *Geophysics* 75 (6), A53–A56.
- Carcione, J., 2014. Wave Fields in Real Media: Wave Propagation in Anisotropic, Anelastic, Porous and Electromagnetic Media. Elsevier Science.
- Carcione, J.M., Kosloff, D., Kosloff, R., 1988. Wave propagation simulation in a linear viscoacoustic medium. *Geophys. J. Int.* 93 (2), 393–401.
- Carcione, J.M., Kosloff, D., Kosloff, R., 1988. Wave propagation simulation in a linear viscoelastic medium. *Geophys. J. Int.* 95 (3), 597–611.
- Carcione, J.M., Kosloff, D., Kosloff, R., 1988. Wave-propagation simulation in an elastic anisotropic (transversely isotropic) solid. *Q. J. Mech. Appl. Math.* 41 (3), 319–346.
- Carcione, J.M., Cavallini, F., Mainardi, F., Hanyga, A., 2002. Time-domain modeling of constant-Q seismic waves using fractional derivatives. *Pure Appl. Geophys.* 159 (7–8), 1719–1736.
- Carcione, J.M., Morency, C., Santos, J.E., 2010. Computational poroelasticity A review. *Geophysics* 75 (5), 75A229–75A243.
- Carcione, J., Zhu, T., Picotti, S., Gei, D., 2016. Imaging septaria geobody in the boom clay using a Q-compensated reverse-time migration. *Neth. J. Geosci.* 95 (3), 283–291.
- Cormen, T.H., Leiserson, C.E., Rivest, R.L., Stein, C., 2009. Introduction to Algorithms. MIT press.
- Dablain, M., 1986. The application of high-order differencing to the scalar wave equation. *Geophysics* 51 (1), 54–66.
- Etgen, J.T., Dellinger, J., 1989. Accurate wave-equation modeling. In: SEG Technical Program Expanded Abstracts 1989. Society of Exploration Geophysicists, pp. 494–497.
- Fomel, S., Ying, L., Song, X., 2013. Seismic wave extrapolation using lowrank symbol approximation. *Geophys. Prospect.* 61 (3), 526–536.
- Fornberg, B., 1987. The pseudospectral method: comparisons with finite differences for the elastic wave equation. *Geophysics* 52 (4), 483–501.
- Kelly, K., Ward, R., Treitel, S., Alford, R., 1976. Synthetic seismograms: a finite-difference approach. *Geophysics* 41 (1), 2–27.
- Kjartansson, E., 1979. Constant Q-wave propagation and attenuation. *J. Geophys. Res.: Solid Earth* 84 (B9), 4737–4748.
- Kosloff, D.D., Baysal, E., 1982. Forward modeling by a Fourier method. *Geophysics* 47 (10), 1402–1412.
- Kosloff, D., Queiroz Filho, A., Tessmer, E., Behle, A., 1989. Numerical solution of the acoustic and elastic wave equations by a new rapid expansion method. *Geophys. Prospect.* 37 (4), 383–394.
- LeVeque, R.J., 2002. Finite Volume Methods for Hyperbolic Problems, vol. 31, Cambridge university press.
- Mainardi, F., 2010. Fractional Calculus and Waves in Linear Viscoelasticity: an Introduction to Mathematical Models. World Scientific.
- Özdenvar, T., McMechan, G.A., 1996. Causes and reduction of numerical artefacts in pseudo-spectral wavefield extrapolation. *Geophys. J. Int.* 126 (3), 819–828.
- Pestana, R.C., Stoffa, P.L., 2010. Time evolution of the wave equation using rapid expansion method. *Geophysics* 75 (4), T121–T131.
- Pippig, M., 2013. Pfft: an extension of fftw to massively parallel architectures. *SIAM J. Sci. Comput.* 35 (3), C213–C236.
- Podlubny, I., 1998. Fractional Differential Equations: an Introduction to Fractional Derivatives, Fractional Differential Equations, to Methods of Their Solution and Some of Their Applications, vol. 198, Elsevier.
- Pratt, R.G., Worthington, M., 1990. Inverse theory applied to multi-source cross-hole tomography. part 1: acoustic wave-equation method. *Geophys. Prospect.* 38 (3), 287–310.
- Soubaras, R., Zhang, Y., 2008. Two-step explicit marching method for reverse time migration. In: 70th EAGE Conference and Exhibition Incorporating SPE EUROPEC.
- Stein, E., 1999. Harmonic analysis real-variable methods, orthogonality, and oscillatory integrals. *Bull. Am. Math. Soc.* 36, 505–521.
- Štekl, I., Pratt, R.G., 1998. Accurate viscoelastic modeling by frequency-domain finite differences using rotated operators. *Geophysics* 63 (5), 1779–1794.
- Sun, J., Zhu, T., Fomel, S., 2015. Viscoacoustic modeling and imaging using low-rank approximation. *Geophysics* 80 (5), A103–A108.
- Tal-Ezer, H., 1986. Spectral methods in time for hyperbolic equations. *SIAM J. Numer. Anal.* 23 (1), 11–26.
- Tal-Ezer, H., Kosloff, D., Koren, Z., 1987. An accurate scheme for seismic forward modeling. *Geophys. Prospect.* 35 (5), 479–490.

- Zhan, G., Pestana, R.C., Stoffa, P.L., 2012. Decoupled equations for reverse time migration in tilted transversely isotropic media. *Geophysics* 77 (2), T37–T45.
- Zhang, Y., Zhang, G., 2009. One-step extrapolation method for reverse time migration. *Geophysics* 74 (4), A29–A33.
- Zhang, Y., Zhang, H., Zhang, G., 2011. A stable TTI reverse time migration and its implementation. *Geophysics* 76 (3), WA3–WA11.
- Zhu, T., Carcione, J.M., 2013. Theory and modelling of constant-Q P-and S-waves using fractional spatial derivatives. *Geophys. J. Int.* 196 (3), 1787–1795.
- Zhu, T., Harris, J.M., 2014. Modeling acoustic wave propagation in heterogeneous attenuating media using decoupled fractional laplacians. *Geophysics* 79 (3), T105–T116.
- Zhu, T., Harris, J.M., Biondi, B., 2014. Q-compensated reverse-time migration. *Geophysics* 79 (3), S77–S87.

UNCORRECTED PROOF